JOURNAL OF AIRCRAFT
Vol. 43, No. 3, May–June 2006

Engineering Notes

ENGINEERING NOTES are short manuscripts describing new developments or important results of a preliminary nature. These Notes should not exceed 2500 words (where a figure or table counts as 200 words). Following informal review by the Editors, they may be published within a few months of the date of receipt. Style requirements are the same as for regular contributions (see inside back cover).

Numerical Simulation and Physical Characteristics Analysis for Slender Wing Rock

Wei Liu*
National University of Defense Technology of China, 410073 Changsha, People's Republic of China
Hanxin Zhang†
China Aerodynamics Research and Development Center, 621000 Mianyang, People's Republic of China
and
Haiyang Zhao‡
National University of Defense Technology of China, 410073 Changsha, People's Republic of China

I. Introduction

THE high-angle-of-attack flight regime often includes complex phenomena such as unsteady flow, crossflow separation, and vortex breakdown. Modern tactical fighters fly at high angles of attack to take advantage of the nonlinear lift generated by vortices that form on their leeward sides. This results in substantial improvement of an aircraft's maneuver and agility performance. However, at sufficiently high angles of attack, vortex asymmetries can form and lead to a self-sustained lateral oscillation phenomenon known as wing rock. Wing rock may cause serious maneuvering and tracking problems for fighters, degrade weapon aiming accuracy, and cause safety problems during taking off or landing approach.

In 1981, the phenomena of slender wing rock were first investigated in wind-tunnel experiments performed by Nguyen et al.[1] Later, a number of experiments[2–7] have also investigated wing rock for delta wing geometries with single degree of freedom (DOF) in roll. These studies have contributed significantly to the understanding of unsteady vortex-dominated flowfields.

From a computational point of view, considerable effort has also been made to develop methods of predicting wing rock due to the difficulty of model installation for free motion in the tunnel and for better flowfield visualization. Because the flowfield is often unsteady and highly nonlinear, computational fluid dynamics flow simulations can be computationally costly. Some investigators[8–10] coupled the unsteady vortex-lattice method with the rigid-body dynamics in roll to simulate numerically wing rock with extremely low computational cost. Some investigators[11–13] reduced the computational cost by employing the inviscid Euler equations in conical form. Although these simplifications reduce the computational cost, they inherently eliminate prediction of a number of relevant flow features. Among the published papers, only a few works[11,14] predicted wing rock by solving unsteady, full Navier–Stokes equations.

The purpose of this paper is to report the continuing development of a full Navier–Stokes methodology to study unsteady vortex-dominated flows about rolling, highly swept delta wings undergoing free-to-roll motions. Although this approach is more computationally costly, it contains all of the relevant flow physics. The flow solver of the code involves a space third-order-accurate weighted nonoscillatory, containing no free parameters and dissipative (WNND) scheme.[15] The code was developed to allow for the analysis of the free-to-roll case by including the rigid-body equation of motion for its simultaneous time integration of the governing flow equations. Results are presented for a 80-deg swept sharp-leading-edge delta wing at 10-, 22-, and 30-deg angle of attack AOA in a freestream of Mach number 0.35. The results give insight into the flow physics associated with unsteady vertical flows about free-to-roll delta wings.

II. Numerical Approach

A. Governing Equations

The flow is governed by the time-dependent full three-dimensional Navier–Stokes equations. The motion of free-to-roll delta wing is governed by the single-DOF Euler equation of rigid-body dynamics. The nondimensional equations are

$$\frac{\partial \bar{U}}{\partial t} + \frac{\partial \bar{\boldsymbol{E}}}{\partial \xi} + \frac{\partial \bar{\boldsymbol{F}}}{\partial \eta} + \frac{\partial \bar{\boldsymbol{G}}}{\partial \varsigma} = \frac{\partial \bar{\boldsymbol{E}}_v}{\partial \xi} + \frac{\partial \bar{\boldsymbol{F}}_v}{\partial \eta} + \frac{\partial \bar{\boldsymbol{G}}_v}{\partial \varsigma} \tag{1}$$

$$\ddot{\phi} = C_1 C_l + C_2 \dot{\phi} \tag{2}$$

where $\bar{U}$ is the vector of conserved variables, and $\bar{\boldsymbol{E}}$, $\bar{\boldsymbol{F}}$, and $\bar{\boldsymbol{G}}$ are the inviscid flux vectors in the ξ, η, and ζ directions, respectively. $\bar{\boldsymbol{E}}_v$, $\bar{\boldsymbol{F}}_v$, and $\bar{\boldsymbol{G}}_v$ are the viscid flux vectors in the ξ, η, and ζ directions, respectively, and ϕ is the roll angle, which is positive clockwise when viewed from aft. C_l is the aerodynamic rolling-moment coefficient about the longitudinal axis. C_1 and C_2 are nondimensional coefficients defined as $C_1 = \rho_\infty S c^3/(2I_{xx})$ and $C_2 = \mu_x c/(I_{xx} V_\infty)$. I_{xx} is the mass moment of inertia about longitudinal axis, and μ_x is a structural damping. S is the planform area, and c is root chord of wing.

B. Solution Algorithm

The flow solver of the code involves a space third-order-accurate WNND scheme.[15] Here, one-dimension hyperbolic conservation laws are used to illuminate the scheme,

$$\frac{\partial U}{\partial t} + \frac{\partial \boldsymbol{F}}{\partial x} = 0 \tag{3}$$

Presented as Paper 2005-4724 at the AIAA 23rd Applied Aerodynamics Conference, Toronto, ON, 6–9 June 2005; received 2 July 2005; revision received 24 September 2005; accepted for publication 26 September 2005.

*Associate Professor, College of Aerospace and Material Engineering; fishfather6525@sina.com.
†Academician of Science, Institute of Computational Aerodynamics.
‡Graduate Student, College of Aerospace and Material Engineering; zhao_haiy@tom.com.

The semidiscretized form of Eq. (3) by employing WNND scheme of three-order-accurate in space can be written as follows:

$$\left(\frac{\partial U}{\partial t}\right)_i = -\frac{1}{\Delta x}\left(\widehat{F}_{i+\frac{1}{2}} - \widehat{F}_{i-\frac{1}{2}}\right) \tag{4}$$

where

$$\widehat{F}_{i+\frac{1}{2}} = \tfrac{1}{2}(F_i + F_{i+1}) + \tfrac{1}{2}\left(A^+_{i+\frac{1}{2}} H^L_{i+\frac{1}{2}} - A^-_{i+\frac{1}{2}} H^R_{i+\frac{1}{2}}\right)$$

$$H^L_{i+\frac{1}{2}} = -\Delta U_{i+\frac{1}{2}} + \omega^+_1 \Delta_{i-\frac{1}{2}} U + \omega^+_0 \Delta_{i+\frac{1}{2}} U$$

$$H^R_{i+\frac{1}{2}} = -\Delta U_{i+\frac{1}{2}} + \omega^-_1 \Delta_{i+\frac{1}{2}} U + \omega^-_0 \Delta_{i+\frac{3}{2}} U$$

$$\omega^\pm_i = \alpha^\pm_i \Big/ \left(\sum_{j=0}^{1} \alpha^\pm_j\right), \qquad \alpha^\pm_i = c^\pm_i \Big/ \left(\varepsilon + IS^\pm_i\right)^2, (i = 0, 1)$$

$$c^+_0 = \tfrac{2}{3}, \qquad c^+_1 = \tfrac{1}{3}, \qquad c^-_0 = \tfrac{1}{3}, \qquad c^-_1 = \tfrac{2}{3}$$

For time integration of Eq. (3), the alternating-direction implicit method is employed to enhance the calculation efficiency for steady-state calculations, and the dual-time-step method, which is a Newton-like subiteration process, is employed to reduce the effect of the inherent time lag in applying the boundary conditions and to reduce the factorization error for unsteady-state calculations.

The rigid-body dynamics equation (2) is solved by using a time second-order-accurate finite difference scheme[12] as

$$\phi^{n+1} = k_1\phi^n + k_2\phi^{n-1} + k_3\phi^{n-2} + k_4 \tag{5}$$

where

$$k_1 = \frac{10 + 4\Delta t C_2}{4 + 3\Delta t C_2}, \qquad k_2 = -\frac{8 + \Delta t C_2}{4 + 3\Delta t C_2}$$

$$k_3 = \frac{2}{4 + 3\Delta t C_2}, \qquad k_4 = \frac{2\Delta t^2 C^{n+1}_l C_1}{4 + 3\Delta t C_2}$$

Because the wing is undergoing rolling motion, a moving grid is generated by moving a static grid with the same angular motion as that of the wing, which satisfies the geometric conservation law strictly ($\partial J^{-1}/\partial t \equiv 0$). The dynamic boundary condition, $\partial p/\partial n$, on the wing surface for the oscillating wing is $\partial p/\partial n = -\rho \boldsymbol{a}_w \cdot \boldsymbol{n}_w$. The boundary condition of temperature is obtained from the adiabatic boundary condition. At the inflow boundaries, the Riemann-invariant boundary-type conditions are enforced. At the outflow boundaries, first-order extrapolation from the interior points is used because the distance between the tail of the wing and the out boundary is as long as five-chord lengths.

III. Results and Discussion

The model geometry consists of an 80-deg swept, sharp-edged delta wing. An O–H grid of $73 \times 77 \times 47$ in the axial, wraparound, and normal directions, respectively, is used. The computational domain extends two and one-half chord lengths forward and five-chord lengths backward from the wing tailing edge. The initial conditions hold at 10-, 22-, and 30-deg AOA at Mach number 0.35 and a Reynolds number of 2.5×10^6. The frictional damping μ_x is set to zero through a simulating process. The mass moment of inertia I_{xx} is 0.1218×10^{-4} kg · m^2.

From the initial conditions, the flow is first solved for the stationary wing at 0-deg roll angle. Then, the wing is forced to roll to an initial roll angle of 10 deg. Finally, the wing is released to roll in response to the flowfield. Figure 1 shows the time history of the resultant motion at 10-, 22-, and 30-deg AOA. After the initial

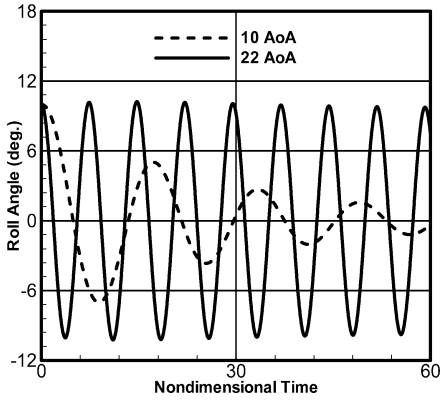

a) 10- and 22-deg AOA

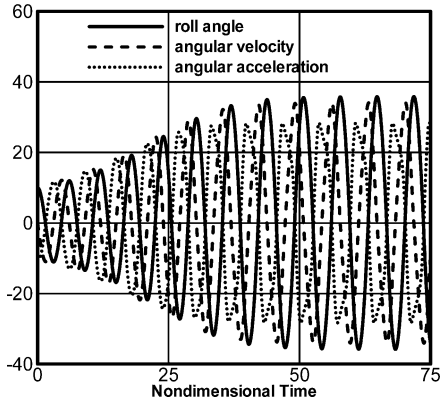

b) 30-deg AOA

Fig. 1 Influence of AOA on free-to-roll response at $M_\infty = 0.35$.

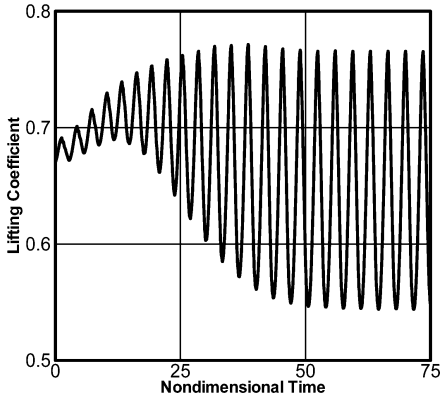

Fig. 2 Lifting coefficient response at 30-deg AOA.

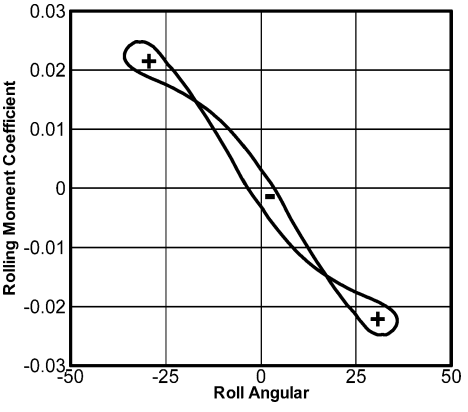

Fig. 3 Hysteresis response at 30-deg AOA.

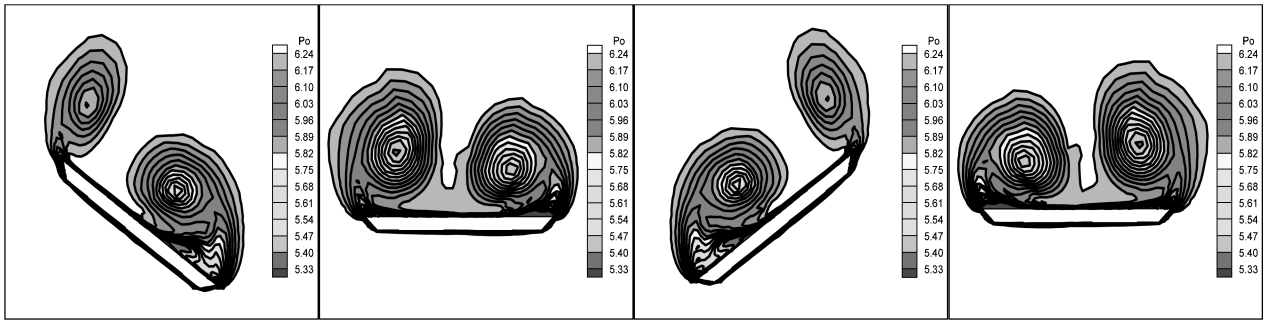

a) $\phi = 35.8$, $\dot{\phi} = 0.0$ b) $\phi = 0.00$, $\dot{\phi} < 0.0$ c) $\phi = -35.8$, $\dot{\phi} = 0.0$ d) $\phi = 0.00$, $\dot{\phi} > 0.0$

Fig. 4 Total-pressure contours during wing rock cycle, $\alpha = 30$ deg and $x/c = 0.62$.

perturbation, the roll oscillatory response converges fast to its initial steady-state value for the positive aerodynamic damping at 10-deg AOA (Fig. 1a). Because the positive aerodynamic damping is so small at 22-deg AOA, the oscillating wing converges very slowly (Fig. 1a). Figure 1b shows the time history of roll angle, angular velocity, and angular acceleration at 30-deg AOA. The wing oscillated in roll with growing amplitude until periodicity is reached seven cycles later. The motion is completely periodic with a maximum limit-cycle amplitude of 35.82 deg, which is 37.8 deg in Nguyen's experiment[1] and 35.5 in the Ng et al. experiment.[3] When wing rock occurs, it is clear that the angular acceleration and roll angle are exactly 180-deg out of phase, whereas the angular velocity and roll angle are nearly 90-deg out of phase.

Figure 2 is the time history of lift coefficient at 30-deg AOA and shows that the curves of the lift coefficient oscillate at twice frequency of the wing motion. In fact, when wing rock occurs, all longitudinal aerodynamic forces/moments oscillate at twice the frequency of the lateral aerodynamic forces/moments. Figure 3 shows the hysteresis loops of the rolling moment coefficient. The hysteresis loops of the rolling moment coefficient show a double 8 style. These lobes represent the energy shift from the wing to the fluid in the outer two lobes (as indicated by the $+$), which are counterclockwise, and from the fluid to the wing in the middle lobe (as indicated by the $-$), which is clockwise. The area of the clockwise lobe is equal to counterclockwise lobes, which means that the total energy of aerodynamic force acted on the wing is equal to zero in a period.

Figures 4a–4d are the total-pressure contours on crossflow planes ($x/c = 0.62$) during a cycle of wing rock. They show the moving positions of the vortex core in a period. When the roll angle is small, the distance between the vortex core and the upward moving wing side decreases and the sucking action of the vortex core increases. The other side of the oscillating wing is in opposition. They create an unsteady rolling moment to enlarge the roll angle. When the roll angle continues increasing, the vortex core moves out of the upward moving wing side; which decreases the region of the sucking action of the vortex core. At the same time, the vortex core moves inside at the downward moving wing-side and produces a resume moment to make the wing roll in the opposite direction. The process is like an aerodynamic spring. In fact, the physical mechanism of wing rock is complex. The liftoff and reattachment of the leading-edge vortex is one cause of wing rock. The wing rock of an 80-deg swept wing is of this type, and it is validated again in this paper.

The numerical results of the wing rock study show that when the AOA increases to about 22 deg Hopf bifurcation of the delta wing occurs and that the equilibrium point becomes the periodic attractor from a stable focus (when $\alpha < 22$ deg) in-phase plane. The onset AOA of wing rock are 27 deg in Nguyen's experiment[1] and 22.8 deg in the Ng et al. experiment.[3] It is reasonable that the onset angle AOA of wing rock in this paper is smaller than that in experiments because the rolling frictional damping is set to zero in the numerical simulation.

IV. Conclusions

The unsteady, compressible, full Navier–Stokes equations and Euler equations of rigid-body dynamics are coupled to simulate the wing rock phenomenon of an 80-deg swept, sharp-edged, delta wing at Mach number 0.35. The numerical results show that 22 deg is the onset AOA of wing rock for the 80-deg swept, sharp-edged delta wing. When the AOA is less than 22 deg, the free-to-roll motion of the disturbed delta wing will converge to the equilibrium position. When the AOA is greater than 22 deg, the free-to-roll motion of the disturbed delta wing will diverge at first and then reach the limit-cycle response.

The phenomena of wing rock shows the following physical characteristics: The angular acceleration and roll angle are nearly 180-deg out of phase, whereas the angular velocity is nearly 90-deg out of phase. The hysteresis loops of the rolling moment coefficient are double 8 style. The area of the clockwise lobe is equal to the counterclockwise lobes, which means that the total energy of aerodynamic force acted on the wing is equal to zero during a period. The physical mechanism of maintaining the wing rock for the 80-deg swept delta wing is liftoff and reattachment of the leading-edge vortex.

References

[1]Nguyen, L. E., Yip, L. P., and Chambers, J. R., "Self-Induced Wing Rock of Slender Delta Wings," AIAA Paper 81-1883, Aug. 1981.

[2]Levin, D., and Katz, J., "Dynamic Load Measurements with Delta Wing Undergoing Self-Induced Roll Oscillations," *Journal of Aircraft*, Vol. 21, No. 1, 1984, pp. 30–36.

[3]Ng, T. T., Malcolm, G. N., and Lewis, L. C., "Experimental Study of Vortex Flows over Delta Wings in Wing-Rock Motion," *Journal of Aircraft*, Vol. 29, No. 4, 1992, pp. 598–603.

[4]Arena, A. J., and Nelson, R. C., "Experimental Investigations on Limit Cycle Wing Rock of Slender Wing," *Journal of Aircraft*, Vol. 31, No. 5, 1994, pp. 1148–1155.

[5]Ericsson, L. E., "Slender Wing Rock Revisited," *Journal of Aircraft*, Vol. 30, No. 3, 1993, pp. 352–356.

[6]Ericsson, L. E., "Wing Rock Analysis of Slender Delta Wings, Review and Extension," *Journal of Aircraft*, Vol. 32, No. 6, 1995, pp. 1221–1226.

[7]Tang, M., Wang, T., Zhang, W., and Xu, Z., "Low Speed Experimental Investigation on Wing Rock," *Acta Aerodynamica Sinica*, Vol. 15, No. 4, 1997, pp. 436–443 (in Chinese).

[8]Konstadinopoulos, P., Mook, D. T., and Nayfeh, A. H., "Subsonic Wing Rock of Slender Delta Wings," *Journal of Aircraft*, Vol. 22, No. 3, 1985, pp. 223–228.

[9]Arena, J. A., and Nelson, R. A., "A Discrete Vortex Model for Predicting Wing Rock of Slender Wings," AIAA Paper 92-4497, Aug. 1992.

[10]Gainer, T. G., "A Discrete-Vortex Method for Studying the Wing Rock of Delta Wings," NASA TP-2002-211965, Dec. 2002.

[11]Kandil, O. A., and Salman, A. A., "Prediction and Control of Slender Wing Rock," International Council of Aeronautical Sciences, ICAS Paper 92-4.7.2, Sept. 1992.

[12]Lee, E. M., and Batina, J. T., "Conical Euler Simulations of Wing Rock for a Delta Wing Planform," *Journal of Aircraft*, Vol. 28, No. 1, 1991, pp. 94–96.

[13]Yang, G. W., Lu, X. Y., and Zhang, L. X., "Nonlinear Analysis of Dynamic Stability and the Prediction of Wing Rock," *Journal of Aircraft,* Vol. 39, No. 1, 2002, pp. 84–90.

[14]Kandil, O. A., and Menzies, M. A., "Effective Control of Computationally Simulated Wing Rock in Subsonic Flow," AIAA Paper 97-0831, Jan. 1997.

[15]Liu, W., Zhao, H., Xie, Y., and Zhang, H., "High-Order WNND Scheme and Its Application in Topological Structure Analysis of Hypersonic Flow Around Liftbody," AIAA Paper 2005-5250, June 2005.